

# Weierstraß-Institut für Angewandte Analysis und Stochastik

im Forschungsverbund Berlin e. V.

Preprint

ISSN 0946 – 8633

## Properties of the steady state distribution of electrons in semiconductors

Orazio Muscato,<sup>1</sup> Wolfgang Wagner<sup>2</sup> and Vincenza Di Stefano<sup>3</sup>

submitted: September 20, 2010

<sup>1</sup> Dipartimento di Matematica e Informatica  
Università degli Studi di Catania  
Viale Andrea Doria 6  
95125 Catania, Italy  
E-Mail: muscato@dmi.unict.it

<sup>2</sup> Weierstrass Institute for  
Applied Analysis and Stochastics  
Mohrenstrasse 39  
10117 Berlin, Germany  
E-Mail: wagner@wias-berlin.de

<sup>3</sup> Dipartimento di Matematica e Informatica  
Università degli Studi di Catania  
Viale Andrea Doria 6  
95125 Catania, Italy  
E-Mail: vdistefano@dmi.unict.it

No. 1537  
Berlin 2010



---

2000 *Mathematics Subject Classification.* 82D37, 65C05.

*Key words and phrases.* Boltzmann-Poisson equation, semiconductors, electron transport, steady state distribution, Monte Carlo algorithm.

Edited by  
Weierstraß-Institut für Angewandte Analysis und Stochastik (WIAS)  
Mohrenstraße 39  
10117 Berlin  
Germany

Fax: +49 30 2044975  
E-Mail: [preprint@wias-berlin.de](mailto:preprint@wias-berlin.de)  
World Wide Web: <http://www.wias-berlin.de/>

## Abstract

This paper studies a Boltzmann transport equation with several electron-phonon scattering mechanisms, which describes the charge transport in semiconductors. The electric field is coupled to the electron distribution function via Poisson's equation. Both the parabolic and the quasi-parabolic band approximations are considered. The steady state behaviour of the electron distribution function is investigated by a Monte Carlo algorithm. More precisely, several nonlinear functionals of the solution are calculated that quantify the deviation of the steady state from a Maxwellian distribution with respect to the wave-vector. On the one hand, the numerical results illustrate known theoretical statements about the steady state and indicate possible directions for future studies. On the other hand, the nonlinear functionals provide tools that can be used in the framework of Monte Carlo algorithms for detecting regions in which the steady state distribution has a relatively simple structure, thus providing a basis for domain decomposition methods.

## Contents

<b>1</b>	<b>Introduction</b>	<b>2</b>
<b>2</b>	<b>Model</b>	<b>3</b>
<b>3</b>	<b>Steady state</b>	<b>6</b>
3.1	Theoretical results . . . . .	6
3.2	Measuring the deviation from a Maxwellian . . . . .	6
<b>4</b>	<b>Numerical approach</b>	<b>8</b>
4.1	Monte Carlo algorithm . . . . .	8
4.2	Calculation of nonlinear functionals . . . . .	8
<b>5</b>	<b>Results</b>	<b>10</b>
5.1	Bulk case - zero electric field . . . . .	10
5.1.1	Steady state dependence on initial state . . . . .	11
5.1.2	Steady state dependence on scattering mechanisms	14
5.1.3	Maxwellian steady state . . . . .	16
5.2	Bulk case - steady state dependence on electric field . . . . .	18
5.3	Diode . . . . .	20
<b>6</b>	<b>Comments</b>	<b>23</b>
	<b>References</b>	<b>23</b>

# 1 Introduction

The study of charge transport in semiconductors is of considerable interest in solid state physics and for the design of electron devices ([10, 16]). The semiclassical kinetic formulation is based on Boltzmann transport equations, which describe the time evolution of the distribution  $f(t, x, k)$  of electrons with respect to position  $x$  and wave-vector  $k$ . These kinetic equations provide the basis for detailed Monte Carlo simulations of charge transport in submicron devices ([8, 5]). In this paper we study a Boltzmann transport equation with several electron-phonon scattering mechanisms, where the electric field is coupled to the electron distribution function via Poisson's equation. Both the parabolic and the quasi-parabolic band approximations are considered.

The purpose of the paper is to study the steady state behaviour ( $t \rightarrow \infty$ ) of the electron distribution function  $f$ . More precisely, we consider several nonlinear functionals of  $f$  that quantify the deviation of the steady state from a Maxwellian distribution with respect to the wave-vector. These functionals are calculated numerically using a Monte Carlo algorithm for the numerical treatment of the Boltzmann transport equation. The motivation for this research is twofold. On the one hand, the numerical results illustrate known theoretical statements about the steady state and indicate possible directions for future studies. On the other hand, the nonlinear functionals provide tools that can be used in the framework of Monte Carlo algorithms for detecting regions in which the steady state distribution has a relatively simple structure. This is of interest for domain decomposition methods and for modelling certain kinds of boundary conditions more efficiently.

The paper is organized as follows. Details of the mathematical model are provided in Section 2. Results concerning the steady state of the electron distribution function are discussed in Section 3. The numerical algorithm is presented in Section 4. The main results are given in Section 5. First the bulk case with zero electric field is investigated. The dependence of the steady state on the initial state and on the scattering mechanisms is illustrated. Then the steady state dependence on the electric field is considered. Finally, in a simple one-dimensional device, the boundary regions are studied where the steady state is determined by the bulk results. Comments and an outlook to future research are given in Section 6.

## 2 Model

In this paper we study the equation

$$\left[ \frac{\partial}{\partial t} + \left( \frac{1}{\hbar} \nabla_k \varepsilon(k) \right) \cdot \nabla_x - \frac{q}{\hbar} E(t, x) \cdot \nabla_k \right] f(t, x, k) = (Qf)(t, x, k), \quad (2.1)$$

which describes the time evolution of the distribution  $f(t, x, k)$  of electrons with respect to position  $x$  and wave-vector  $k$ . The electric field is defined as

$$E(t, x) = -\nabla_x \Phi(t, x), \quad (2.2)$$

where the electric potential  $\Phi$  satisfies the *Poisson equation*

$$\varepsilon \Delta_x \Phi(t, x) = q [n(t, x) - n_D(x)] \quad (2.3)$$

and the electron density

$$n(t, x) = \int_{\mathbb{R}^3} f(t, x, k) dk \quad (2.4)$$

depends on the solution  $f$ . In (2.3), the function  $n_D$  denotes the donor density,  $q$  is the absolute value of the electron charge and  $\varepsilon$  is the permittivity. Boundary conditions to (2.3) take into account an external field. Boundary conditions to (2.1) are more complicated. In the one-dimensional case considered later we will assume periodic boundaries.

We consider analytic bands in the *quasi-parabolic* approximation, where the kinetic energy  $\varepsilon(k)$  of an electron satisfies the relation

$$\varepsilon(k) [1 + \alpha \varepsilon(k)] = \frac{\hbar^2 |k|^2}{2m^*}, \quad k \in \mathbb{R}^3. \quad (2.5)$$

Here  $\alpha$  denotes the non-parabolicity factor (the case  $\alpha = 0$  is called *parabolic*),  $m^*$  is the effective electron mass,  $\hbar$  denotes Planck's constant divided by  $2\pi$  and  $\mathbb{R}^3$  is the Euclidean space. According to (2.5), the electron group velocity (cf. (2.1)) takes the form

$$v(k) = \frac{1}{\hbar} \nabla_k \varepsilon(k) = \frac{\hbar k}{m^* [1 + 2\alpha \varepsilon(k)]}, \quad (2.6)$$

where, for  $\alpha > 0$ ,

$$\varepsilon(k) = \frac{\sqrt{1 + \frac{2\alpha \hbar^2 |k|^2}{m^*}} - 1}{2\alpha}.$$

We consider the *linear scattering* collision operator

$$(Qf)(t, x, k) = \int_{\mathbb{R}^3} S(k', k) f(t, x, k') dk' - \lambda(k) f(t, x, k), \quad (2.7)$$

where

$$\lambda(k) = \int_{\mathbb{R}^3} S(k, k') dk' \quad (2.8)$$

is the total scattering rate. The main scattering mechanisms in silicon, at room temperature, are due to electron-phonon interactions (acoustic and optical). The transition rate from a state  $k$  to a state  $k'$  is modelled as (cf. [9, Section III.D.1])

$$S(k, k') = S_{\text{ac}}(k, k') + S_{\text{opt}}(k, k'), \quad (2.9)$$

where

$$S_{\text{ac}}(k, k') = K_0 \delta(\varepsilon(k') - \varepsilon(k)) \quad (2.10)$$

and

$$S_{\text{opt}}(k, k') = \sum_{i=1}^6 K_i \left[ \delta(\varepsilon(k') - \varepsilon(k) + \hbar\omega_i) (n_{q_i} + 1) + \delta(\varepsilon(k') - \varepsilon(k) - \hbar\omega_i) n_{q_i} \right]. \quad (2.11)$$

The coefficients are (cf. Tables 1, 2)

$$K_0 = \frac{k_B T_L \Xi_d^2}{4\pi^2 \hbar \rho v_s^2}$$

and

$$K_i = \frac{(D_t K)_i^2 Z_i}{8\pi^2 \rho \omega_i}, \quad i = 1, \dots, 6.$$

The quantities  $\hbar\omega_i$  in (2.11) are phonon energies. The phonon occupation numbers are defined as

$$n_{q_i} = \frac{1}{\exp(\hbar\omega_i/k_B T_L) - 1},$$

where  $k_B$  denotes Boltzmann's constant and  $T_L$  is the lattice temperature. We refer to [8, Section 2.2.5] for further details of the modelling.

The operator (2.7) has a simple probabilistic interpretation. The term (2.10) corresponds to acoustic scattering (elastic approximation), which means that the energy of the electron is preserved and it just gets a new orientation. The term (2.11) corresponds to optical scattering (six branches, inelastic), which means that the electron either loses energy (interpreted as emission of a phonon) or gains energy (interpreted as absorption of a phonon). Emission of a phonon is only possible if  $\varepsilon(k) < \hbar\omega_i$ , otherwise the electron does not have enough energy. Note that (cf. (2.8), (2.9))

$$\lambda(k) \sim \sqrt{\varepsilon(k)} \sqrt{1 + \alpha \varepsilon(k)} (1 + 2\alpha \varepsilon(k)) \quad \text{as } |k| \rightarrow \infty,$$

which implies  $\lambda(k) \sim |k|$  (parabolic case) and  $\lambda(k) \sim |k|^2$  (quasi-parabolic case).

$m_e$	electron rest mass	$9.1095 \cdot 10^{-28} \text{ g}$
$m^*$	effective mass	$0.3216 m_e$
$\rho$	mass density	$2.33 \text{ g/cm}^3$
$v_s$	longitudinal sound speed	$9.18 \cdot 10^5 \text{ cm/sec}$
$\Xi_d$	acoustic phonon deformation potential	$9 \text{ eV}$
$\alpha$	non-parabolicity factor	$0.5 \text{ eV}^{-1}$

Table 1: Silicon parameters

$i$	scattering (branch)	$\hbar\omega_i(\text{meV})$	$(D_t K)_i (\text{eV \AA}^{-1})$	$Z_i$
1	g-1 (TA)	12	0.5	1
2	g-2 (LA)	18.5	0.8	1
3	g-3 (LO)	61.2	11	1
4	f-1 (TA)	19.0	0.3	4
5	f-2 (LA)	47.4	2.0	4
6	f-3 (TO)	59.0	2.0	4

Table 2: Coupling constants for optical phonon scattering

### spatially homogeneous case

If the initial state is spatially homogeneous, i.e.,

$$f(0, x, k) = f_0(k) \quad \forall x$$

and the doping density (cf. (2.3)) satisfies

$$n_D(x) = \int_{\mathbb{R}^3} f_0(k) dk \quad \forall x,$$

then equation (2.1) takes the form

$$\left[ \frac{\partial}{\partial t} - \frac{q}{\hbar} E \cdot \nabla_k \right] f(t, k) = (Qf)(t, k), \quad (2.12)$$

where  $E$  is the external field.

### 3 Steady state

#### 3.1 Theoretical results

Convergence of the solution of equation (2.12) to the steady state has been studied in [12]. When assuming zero electric field and one inelastic scattering mechanism, but rather general  $\varepsilon(k)$ , the steady state is characterized as

$$f(k) = f_M(\varepsilon(k))P(\varepsilon(k)),$$

where

$$f_M(k) = A \exp\left(-\frac{\varepsilon(k)}{k_B T_L}\right) \quad (3.1)$$

and  $P$  is a periodic function, that is

$$P(u + \hbar \omega) = P(u) \quad \forall u \geq 0.$$

More results and further references related to equation (2.1) can be found in [13], [2], [1], [3, Ch. 10].

#### 3.2 Measuring the deviation from a Maxwellian

A Maxwell distribution is defined as

$$M_{V,T}(z) = \frac{1}{(2\pi T)^{3/2}} \exp\left(-\frac{|z-V|^2}{2T}\right) \quad z \in \mathbb{R}^3, \quad (3.2)$$

where  $V \in \mathbb{R}^3$  and  $T > 0$  are parameters. Note that (3.1) is a Maxwellian distribution (in the sense of (3.2)) only in the parabolic case (cf. (2.5)).

Let  $\xi$  be an arbitrary three-dimensional random vector and  $\mathbb{E}$  denote mathematical expectation. We consider the functionals

$$\mathbf{kurt}(\xi) = \frac{3}{5} \frac{\mathbb{E}|\xi - \mathbb{E}\xi|^4}{(\mathbb{E}|\xi - \mathbb{E}\xi|^2)^2} \quad (3.3)$$

and

$$\mathbf{crit}(\xi) = \frac{1}{T(\xi)} \left\{ \frac{1}{2} \|\tau(\xi)\|_F^2 + \frac{2}{5} \frac{|q(\xi)|^2}{T(\xi)} + \frac{1}{120} \frac{\gamma(\xi)^2}{T(\xi)^2} \right\}^{\frac{1}{2}}, \quad (3.4)$$

where

$$T(\xi) = \frac{1}{3} \mathbb{E}|\xi - \mathbb{E}\xi|^2$$



$$\tau(\xi) = \mathbb{E}(\xi - \mathbb{E}\xi)(\xi - \mathbb{E}\xi)' - T(\xi)I \quad (3.5)$$

$$q(\xi) = \frac{1}{2} \mathbb{E}(\xi - \mathbb{E}\xi)|\xi - \mathbb{E}\xi|^2$$

$$\gamma(\xi) = \mathbb{E}|\xi - \mathbb{E}\xi|^4 - 15T(\xi)^2.$$

The subscript  $F$  in (3.4) indicates the Frobenius norm of a matrix. The symbol  $I$  in (3.5) denotes the identity matrix and the notation  $zz'$  is used for the matrix with elements  $z_i z_j$ , where  $z \in \mathbb{R}^3$ .

**Remark 3.1** *If  $\xi$  has an arbitrary Maxwellian distribution (3.2), then*

$$\mathbf{kurt}(\xi) = 1 \quad \text{and} \quad \mathbf{crit}(\xi) = 0. \quad (3.6)$$

*Indeed, if  $\xi$  is distributed according to the Maxwellian  $M_{0,1}$ , then  $\mathbb{E}|\xi|^2 = 3$  and  $\mathbb{E}|\xi|^4 = 15$  so that  $T(\xi) = 1$  and  $\tau(\xi) = q(\xi) = \gamma(\xi) = 0$ . Thus, (3.6) is satisfied. The general case follows from the properties*

$$\mathbf{kurt}(\xi + c) = \mathbf{kurt}(\xi), \quad \mathbf{crit}(\xi + c) = \mathbf{crit}(\xi) \quad \forall c \in \mathbb{R}^3$$

and

$$\mathbf{kurt}(c\xi) = \mathbf{kurt}(\xi), \quad \mathbf{crit}(c\xi) = \mathbf{crit}(\xi) \quad \forall c \neq 0.$$

*If  $\xi$  is distributed uniformly on the unit sphere, then*

$$\mathbf{kurt}(\xi) = 0.6. \quad (3.7)$$

The functionals (3.3), (3.4) can be used to “measure” the deviation of a given distribution from a Maxwellian (3.2). The functional (3.3) is a three-dimensional version of the “kurtosis” of a random variable, which is defined as the centered fourth moment normalized by the fourth power of the standard deviation and is interpreted as the “degree of peakedness”. A functional of the form

$$\frac{3}{5} \frac{\mathbb{E}\varepsilon(k)^2}{(\mathbb{E}\varepsilon(k))^2} \quad (3.8)$$

was used in [6, 7] to quantify the deviation from a Maxwellian shape (3.1). The functional (3.8) coincides with (3.3) in the parabolic case (cf. (2.5)) with zero mean value. The functional (3.4) was used in [15, p.148] as a criterion to detect regions where the solution of the Boltzmann equation is close to a Maxwellian.

## 4 Numerical approach

### 4.1 Monte Carlo algorithm

The Monte Carlo approach (cf. [8]) is based on a stochastic particle system of the form

$$\left( x_i(t), k_i(t) \right) \quad i = 1, \dots, N \quad t \geq 0. \quad (4.1)$$

A time step  $\Delta t$  is used to decouple the transport equation (2.1) and the Poisson equation (2.3). That is, each particle moves with its velocity (2.6), performs scatterings according to the rate function (2.9) and is accelerated according to a fixed electric field. After  $\Delta t$ , the density (2.4) is measured and the field is re-calculated according to (2.2), (2.3). The system (4.1) provides a numerical algorithm for equation (2.1) in the sense that *linear functionals* of the solution  $f$  are approximated by averages over the particle system, that is

$$\int_{\Delta x} \int_{\mathbb{R}^3} \varphi(k) f(t, x, k) dk dx \sim \frac{1}{N} \sum_{i: x_i(t) \in \Delta x} \varphi(k_i(t)), \quad (4.2)$$

for some spatial cell  $\Delta x$  and appropriate test functions  $\varphi$ . Convergence with respect to the numerical parameters ( $N \rightarrow \infty$  and  $\Delta t \rightarrow 0$ ) has been studied in [14]. The purpose of the present paper is to study the steady state solution of equation (2.1) by using a Monte Carlo algorithm (4.1). We choose  $\Delta t$  small enough so that the corresponding systematic error is smaller than the bounds for the statistical error provided by confidence intervals. The steady state is approximated by a *time averaging* procedure, that is

$$\int_{\Delta x} \int_{\mathbb{R}^3} \varphi(k) f(\infty, x, k) dk dx \sim \frac{1}{J} \sum_{j=1}^J \Phi(t_j, \Delta x), \quad (4.3)$$

where  $\Phi(t, \Delta x)$  is a notation for the right-hand side of (4.2) and  $t_1, \dots, t_J$  are appropriate observation points (far enough from  $t = 0$ ).

### 4.2 Calculation of nonlinear functionals

The functionals (3.3), (3.4) are considered for a random vector  $\xi = k$  with the distribution (cf. (2.4))

$$\frac{1}{n(t, x)} f(t, x, k). \quad (4.4)$$

They depend on  $f$  in a nonlinear way. In order to apply the Monte Carlo procedures (4.2) (when studying the time evolution) and (4.3) (when studying the steady state), the functionals (3.3), (3.4) are represented via linear functionals of  $f$  with respect to appropriate test functions  $\varphi$ . One obtains

$$\mathbb{E} |\xi - \mathbb{E}\xi|^2 = \mathbb{E} |\xi|^2 - |\mathbb{E}\xi|^2 \quad (4.5)$$

and

$$\mathbb{E}(\xi - \mathbb{E}\xi)(\xi - \mathbb{E}\xi)' = \mathbb{E}\xi\xi' - (\mathbb{E}\xi)(\mathbb{E}\xi)'. \quad (4.6)$$

Moreover,

$$\mathbb{E}(\xi - \mathbb{E}\xi)|\xi - \mathbb{E}\xi|^2 = \mathbb{E}\xi|\xi|^2 - 2\mathbb{E}\xi(\xi, \mathbb{E}\xi) - \mathbb{E}\xi|\mathbb{E}\xi|^2 + 2\mathbb{E}\xi|\mathbb{E}\xi|^2 \quad (4.7)$$

and

$$\mathbb{E}\xi(\xi, \mathbb{E}\xi) = \mathbb{E}\xi\xi'\mathbb{E}\xi. \quad (4.8)$$

Finally,

$$\begin{aligned} \mathbb{E}|\xi - \mathbb{E}\xi|^4 = \\ \mathbb{E}|\xi|^4 + 4\mathbb{E}(\xi, \mathbb{E}\xi)^2 - 3|\mathbb{E}\xi|^4 - 4(\mathbb{E}\xi, \mathbb{E}\xi|\xi|^2) + 2\mathbb{E}|\xi|^2|\mathbb{E}\xi|^2 \end{aligned} \quad (4.9)$$

and

$$\mathbb{E}(\xi, \mathbb{E}\xi)^2 = \left( \mathbb{E}\xi\xi', (\mathbb{E}\xi)(\mathbb{E}\xi)' \right) \quad (4.10)$$

where  $(\cdot, \cdot)$  denotes the scalar product of matrices. Using identities (4.5)-(4.10), the functionals (3.3), (3.4) are represented via the expected values

$$\mathbb{E}\xi, \quad \mathbb{E}|\xi|^2, \quad \mathbb{E}|\xi|^4, \quad \mathbb{E}\xi\xi', \quad \mathbb{E}\xi|\xi|^2$$

and, according to (4.4), in terms of the “primary” quantities

$$\int_{\mathbb{R}^3} \varphi^{(l)}(k) f(t, x, k) dk, \quad l = 0, 1, 2, 3, 4,$$

where

$$\begin{aligned} \varphi^{(0)}(k) = 1, \quad \varphi_i^{(1)}(k) = k_i, \quad \varphi_{i,j}^{(2)}(k) = k_i k_j \\ \varphi_i^{(3)}(k) = k_i |k|^2, \quad \varphi^{(4)}(k) = |k|^4, \quad i, j = 1, 2, 3. \end{aligned} \quad (4.11)$$

Let

$$\begin{aligned} m^{(0)}(t, \Delta x), \quad m_i^{(1)}(t, \Delta x) = k_i, \quad m_{i,j}^{(2)}(t, \Delta x) \\ m_i^{(3)}(t, \Delta x), \quad m^{(4)}(t, \Delta x), \quad i, j = 1, 2, 3 \end{aligned}$$

and

$$\begin{aligned} m^{(0)}(\infty, \Delta x), \quad m_i^{(1)}(\infty, \Delta x) = k_i, \quad m_{i,j}^{(2)}(\infty, \Delta x) \\ m_i^{(3)}(\infty, \Delta x), \quad m^{(4)}(\infty, \Delta x), \quad i, j = 1, 2, 3 \end{aligned}$$

denote the Monte Carlo approximations (right-hand sides of (4.2) and (4.3), respectively) of the integrals of  $f$  with respect to the test functions (4.11). The corresponding values of the functionals (3.3), (3.4) are denoted by  $\text{kurt}(t, \Delta x)$ ,  $\text{crit}(t, \Delta x)$  and  $\text{kurt}(\infty, \Delta x)$ ,  $\text{crit}(\infty, \Delta x)$ , respectively.

In order to construct *confidence intervals*,  $N_{\text{rep}}$  independent runs are performed for each set of parameters. Let  $\eta_r$ ,  $r = 1, \dots, N_{\text{rep}}$ , be realizations of a random quantity (e.g.,  $\text{kurt}(t, \Delta x)$  or  $\text{crit}(\infty, \Delta x)$ ) obtained by independent runs (repetitions). Then the confidence interval is evaluated as

$$\frac{1}{N_{\text{rep}}} \sum_{r=1}^{N_{\text{rep}}} \eta_r \pm 3 \sqrt{\frac{1}{N_{\text{rep}}} \left( \frac{1}{N_{\text{rep}}} \sum_{r=1}^{N_{\text{rep}}} \eta_r^2 - \left[ \frac{1}{N_{\text{rep}}} \sum_{r=1}^{N_{\text{rep}}} \eta_r \right]^2 \right)},$$

where the factor 3 corresponds to a 99.7 % confidence level.

## 5 Results

In this section we investigate the steady state solution of equation (2.1) by means of the numerical algorithm introduced in the previous section. First the spatially homogeneous situation (bulk case) is considered, which corresponds to equation (2.12). Then a spatially one-dimensional test case (diode) is studied.

The steady state is compared with the Maxwellian (3.1) by using the functionals “kurtosis” and “criterion” (cf. (3.3), (3.4)) as well as other macroscopic quantities (e.g., mean energy). Benchmark values are obtained analytically or by numerical integration. Most of them depend on the lattice temperature, which is  $T_L = 300K$ . In the quasi-parabolic case (cf. (2.5)), one obtains

$$\text{kurt}(k) = 1.02578, \quad \mathbb{E} \varepsilon(k) = 0.04000 \text{ eV}, \quad (5.1)$$

while, in the parabolic case,

$$\text{kurt}(k) = 1.0, \quad \mathbb{E} \varepsilon(k) = 0.03878 \text{ eV}. \quad (5.2)$$

Numerical values, obtained by generating independent samples from the distribution (3.1), are given in Table 3. The product of the number of particles and the number of independent repetitions is kept constant,  $N \times N_{\text{rep}} = 10^8$ , so that convergence (with respect to  $N$ ) of the expected values is illustrated. The expectation of the functional  $\text{kurt}(k)$  converges to the values given in (5.1), (5.2). The expectation of the functional  $\text{crit}(k)$  converges to zero in the parabolic case, and to some non-zero quantity in the quasi-parabolic case.

### 5.1 Bulk case - zero electric field

Here we study convergence of the solution of equation (2.1) to the steady state. In particular, we consider the problem whether this steady state is a Maxwellian (3.1).

$N$	kurt( $k$ ), par	kurt( $k$ ), q-par	crit( $k$ ), par	crit( $k$ ), q-par
$10^3$	$0.9993 \pm 0.0002$	$1.0250 \pm 0.0002$	$0.0881 \pm 0.0002$	$0.0975 \pm 0.0002$
$10^4$	$0.9999 \pm 0.0002$	$1.0257 \pm 0.0002$	$0.0279 \pm 0.0002$	$0.0452 \pm 0.0003$
$10^5$	$1.0000 \pm 0.0002$	$1.0257 \pm 0.0002$	$0.0089 \pm 0.0002$	$0.0363 \pm 0.0003$
$10^6$	$1.0000 \pm 0.0002$	$1.0257 \pm 0.0002$	$0.0026 \pm 0.0002$	$0.0354 \pm 0.0003$

Table 3: Numerical values for the functionals (3.3) and (3.4), when  $k$  is distributed according to the Maxwellian (3.1) with  $T_L = 300 K$  (parabolic and quasi-parabolic bands)

The numerical observations illustrate theoretical results and indicate some problems for further studies.

### 5.1.1 Steady state dependence on initial state

We show that different initial states lead to different steady states, as predicted by the theory mentioned in Section 3.1. In order to satisfy the assumptions of the theorem we consider only one scattering mechanism. The parabolic band approximation (cf. (2.5)) is used. The results in the quasi-parabolic case are qualitatively similar.

We consider the scattering mechanism corresponding to  $i = 6$  in Table 2. The initial states are Maxwellians (3.1) with temperatures 270 K, 300 K and 330 K, as well as uniform distributions on the spheres with energies 0.05 eV and 0.045 eV. The parameters  $N = 11000$  and  $N_{\text{rep}} = 100$  are used. The time evolution of the energy, the kurtosis and the criterion is displayed in Figures 1-3.

For all three Maxwellian initial states, no visible deviation from the Maxwellian steady state with the lattice temperature can be detected. Both kurtosis and criterion take their Maxwellian values (1.0 and  $\sim 0.028$ , according to Table 3) at the beginning and the end, and leave them during the time evolution. For initial states with fixed energies, no Maxwellian steady state is reached. The qualitative behaviour of the mean energy can easily be predicted, when taking into account that for the scattering mechanism  $i = 6$  the energy jump is 0.059 eV.

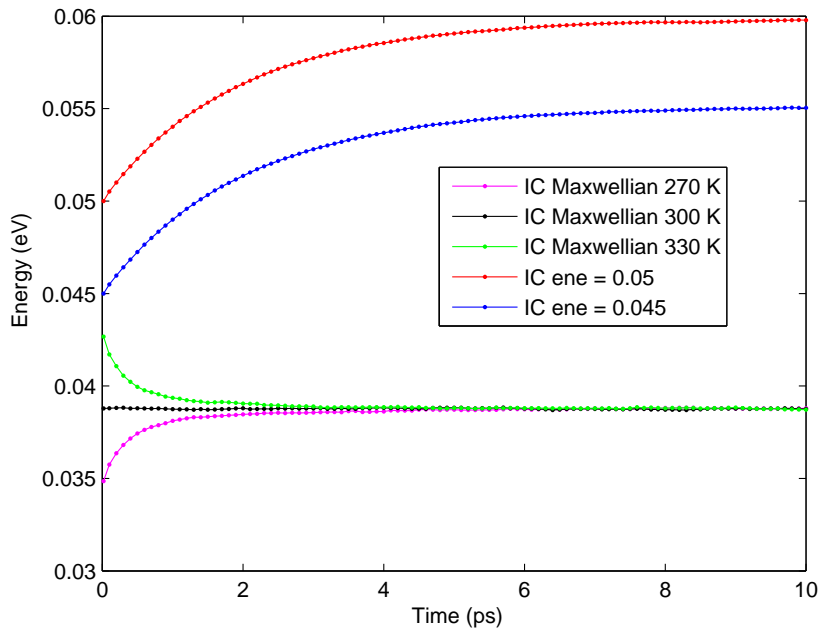


Figure 1: Average energy for different initial states and one scattering mechanism (bulk case, parabolic band, zero electric field)

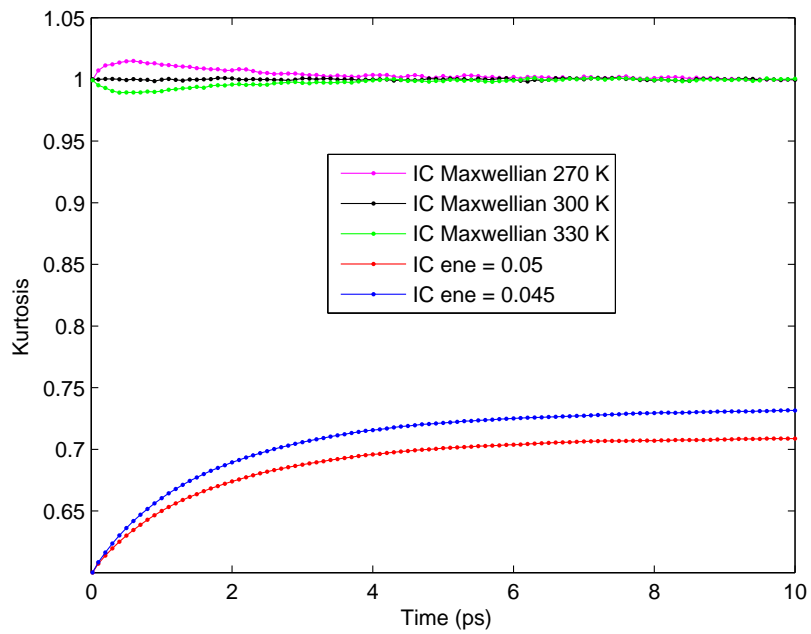


Figure 2: Kurtosis (3.3) for different initial states and one scattering mechanism (bulk case, parabolic band, zero electric field)

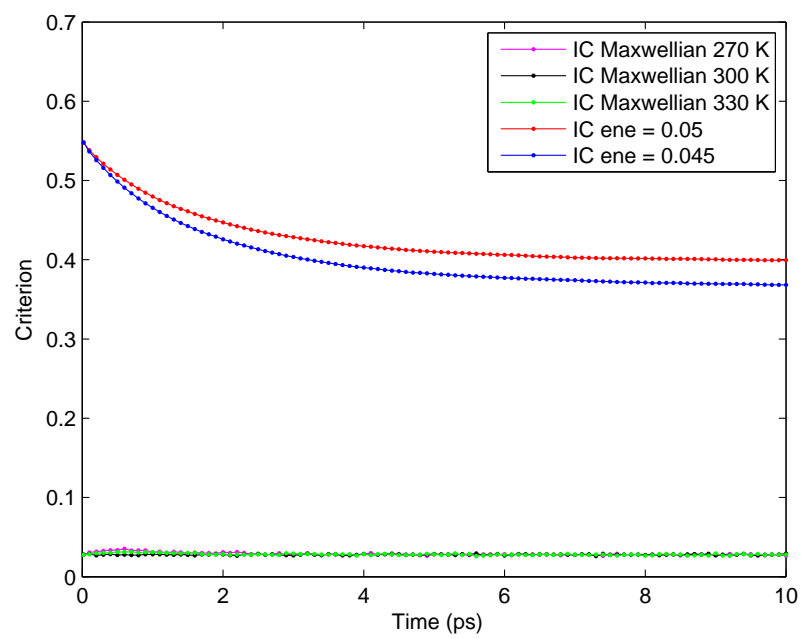


Figure 3: Criterion (3.4) for different initial states and one scattering mechanism (bulk case, parabolic band, zero electric field)

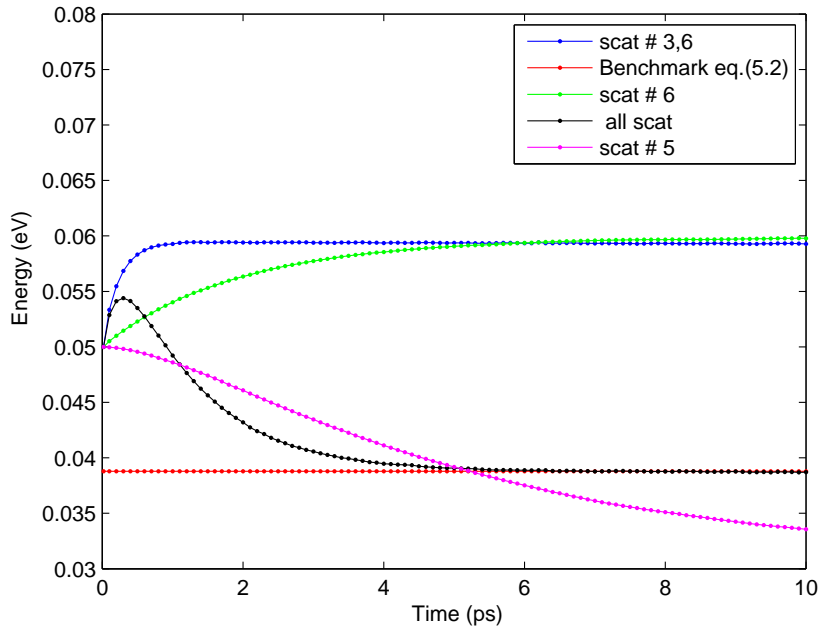


Figure 4: Average energy for a fixed initial state and different scattering mechanisms (bulk case, parabolic band, zero electric field)

### 5.1.2 Steady state dependence on scattering mechanisms

We study the influence of the scattering mechanisms on the steady state. It seems that even the case of two scattering mechanisms is not covered by the theory mentioned in Section 3.1. The parabolic band approximation (cf. (2.5)) is used. The results in the quasi-parabolic case are qualitatively similar.

The initial state is a uniform distribution on the sphere with energy 0.05 eV. Beside the complete set of scattering mechanisms we choose  $i = 6$ ,  $i = 3,6$  and  $i = 5$  (cf. Table 2). The parameters  $N = 11000$  and  $N_{\text{rep}} = 100$  are used. The time evolution of the energy, the kurtosis and the criterion is displayed in Figures 4-6.

The results show that different scattering mechanisms lead to different steady states. However, the combination of all of them seems to imply a Maxwellian steady state uniquely determined by the lattice temperature.



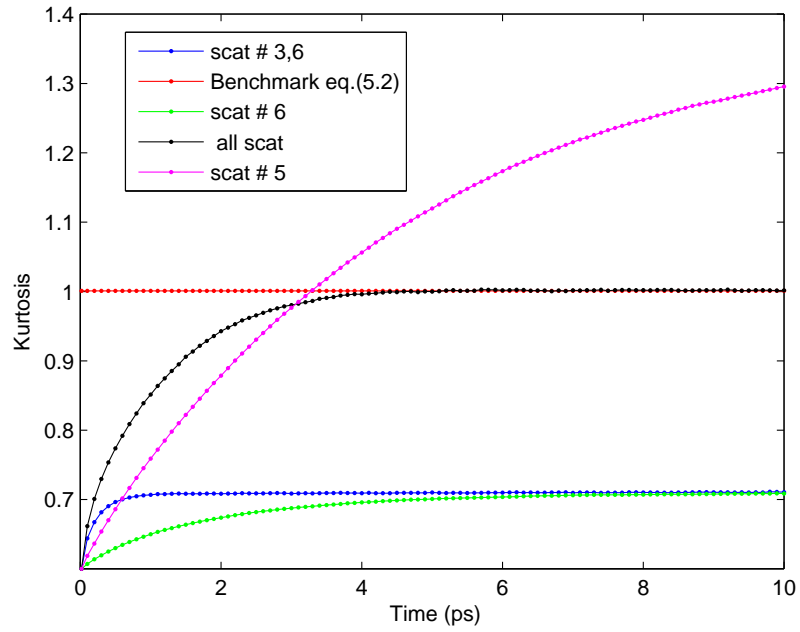


Figure 5: Kurtosis (3.3) for a fixed initial state and different scattering mechanisms (bulk case, parabolic band, zero electric field)

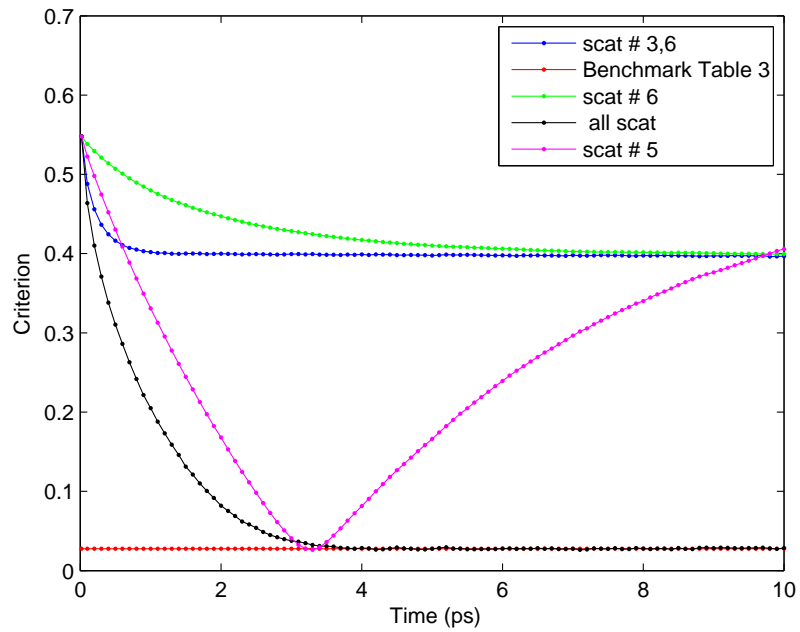


Figure 6: Criterion (3.4) for a fixed initial state and different scattering mechanisms (bulk case, parabolic band, zero electric field)

initial	energy (eV)	kurtosis	criterion
T = 270 K	$0.03999 \pm 0.00001$	$1.0257 \pm 0.0003$	$0.0358 \pm 0.0002$
T = 300 K	$0.03999 \pm 0.00001$	$1.0258 \pm 0.0003$	$0.0354 \pm 0.0002$
T = 330 K	$0.04001 \pm 0.00001$	$1.0256 \pm 0.0003$	$0.0352 \pm 0.0002$
ene = 0.05 eV	$0.03999 \pm 0.00001$	$1.0259 \pm 0.0003$	$0.0356 \pm 0.0002$

Table 4: Steady state values of energy, kurtosis (3.3) and criterion (3.4) for different initial states and all scattering mechanisms (bulk case, quasi-parabolic band, zero electric field)

### 5.1.3 Maxwellian steady state

We include now all scattering mechanisms and illustrate that any initial state leads to the same Maxwellian steady state determined by the lattice temperature. It would be a theoretical challenge to show this rigorously. Both the parabolic and the quasi-parabolic band approximations (cf. (2.5)) are considered. The results in these case are qualitatively similar.

The initial states are Maxwellians (3.1) with temperatures 270 K, 300 K and 330 K, as well as the uniform distribution on the sphere with energy 0.05 eV. The parameters  $N = 10^6$  and  $N_{\text{rep}} = 10$  are used. In addition, the functionals are averaged between 5 ps and 10 ps, with an observation time step of 0.1 ps.

In the quasi-parabolic case, the results for the energy, the kurtosis and the criterion are given in Table 4. They are completely consistent with the data provided by Table 3 so that the steady state is indeed indistinguishable from the Maxwellian determined by the lattice temperature.

In the parabolic case, the time dependent curves for the initial state with fixed energy are contained in Figures 4-6. The time dependent results for the criterion and the Maxwellian initial states are displayed in Figure 7. It is observed that the criterion takes its Maxwellian value ( $\sim 0.003$ , according to Table 3) at the beginning and at the end, while departing from it during the time evolution.

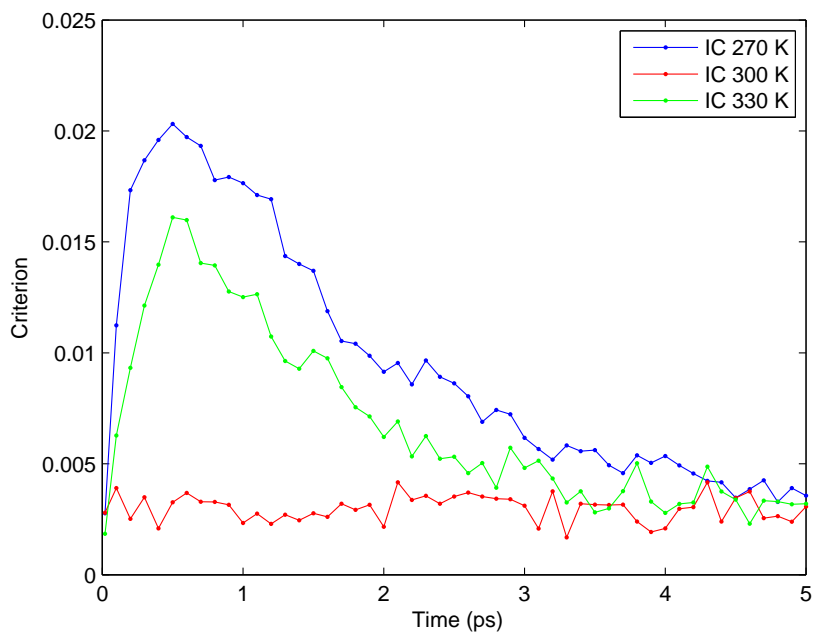


Figure 7: Criterion (3.4) for different initial Maxwellians and all scattering mechanisms (bulk case, parabolic band, zero electric field)

field (V/cm)	energy (eV)	kurtosis	criterion
1	$0.03876 \pm 0.00003$	$0.9998 \pm 0.0006$	$0.0276 \pm 0.0002$
10	$0.03877 \pm 0.00003$	$0.9996 \pm 0.0006$	$0.0278 \pm 0.0002$
100	$0.03878 \pm 0.00003$	$0.9997 \pm 0.0006$	$0.0280 \pm 0.0002$
200	$0.03882 \pm 0.00003$	$0.9996 \pm 0.0006$	$0.0286 \pm 0.0003$
400	$0.03890 \pm 0.00003$	$0.9978 \pm 0.0006$	$0.0307 \pm 0.0003$
800	$0.03922 \pm 0.00003$	$0.9932 \pm 0.0006$	$0.0375 \pm 0.0003$

Table 5: Steady state values of energy, kurtosis (3.3) and criterion (3.4) for Maxwellian initial state and different electric fields (bulk case, parabolic band)

field (V/cm)	energy (eV)	kurtosis	criterion
1000	$0.04058 \pm 0.00003$	$1.0162 \pm 0.0006$	$0.0459 \pm 0.0005$
1300	$0.04092 \pm 0.00003$	$1.0116 \pm 0.0006$	$0.0485 \pm 0.0005$
1400	$0.04105 \pm 0.00004$	$1.0098 \pm 0.0006$	$0.0492 \pm 0.0004$
1500	$0.04116 \pm 0.00003$	$1.0087 \pm 0.0006$	$0.0507 \pm 0.0004$
1600	$0.04129 \pm 0.00003$	$1.0069 \pm 0.0006$	$0.0519 \pm 0.0004$

Table 6: Steady state values of energy, kurtosis (3.3) and criterion (3.4) for Maxwellian initial state and different electric fields (bulk case, quasi-parabolic band)

## 5.2 Bulk case - steady state dependence on electric field

Here we study the dependence of the steady state on the electric field. All scattering mechanisms are included. Both the parabolic and the quasi-parabolic band approximations (cf. (2.5)) are considered.

The initial state is the Maxwellian (3.1) with the lattice temperature, which is the steady state in the case of zero electric field. The parameters  $N = 11000$  and  $N_{\text{rep}} = 100$  are used. The functionals are averaged between 10 ps and 20 ps, with an observation time step of 0.1 ps.

Results for the parabolic case are given in Table 5. They show that a deviation from Maxwellian behaviour can be detected (given the level of statistical fluctuations) for fields between 200 V/cm and 400 V/cm. Table 6 provides some data for the quasi-parabolic case, which will be used for comparisons in the one-dimensional test case. The complete results for the kurtosis and the criterion are displayed in Figures 8 and 9, respectively. They illustrate the deviation of the steady state from the Maxwellian, which becomes apparent for increasing electric fields.

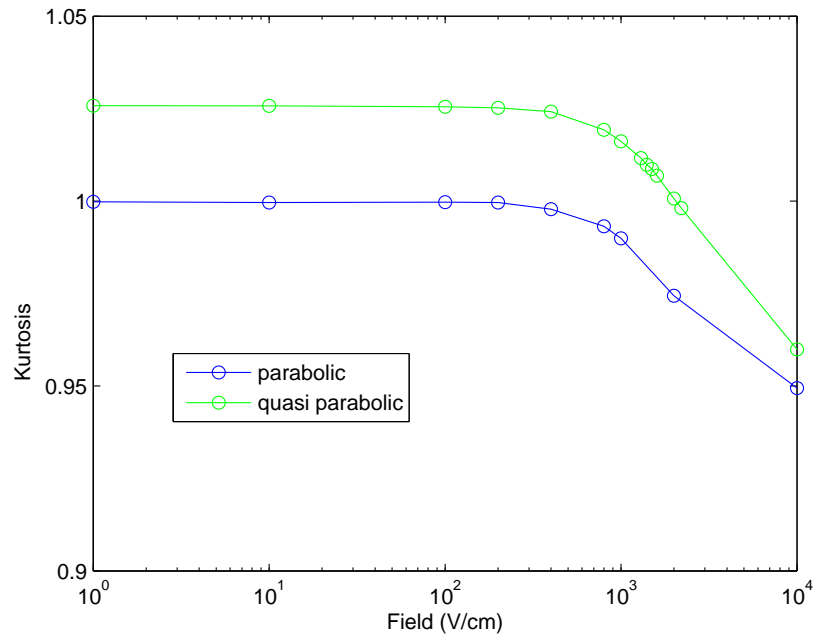


Figure 8: Steady state value of kurtosis (3.3) as a function of the electric field (bulk case, initial Maxwellian)

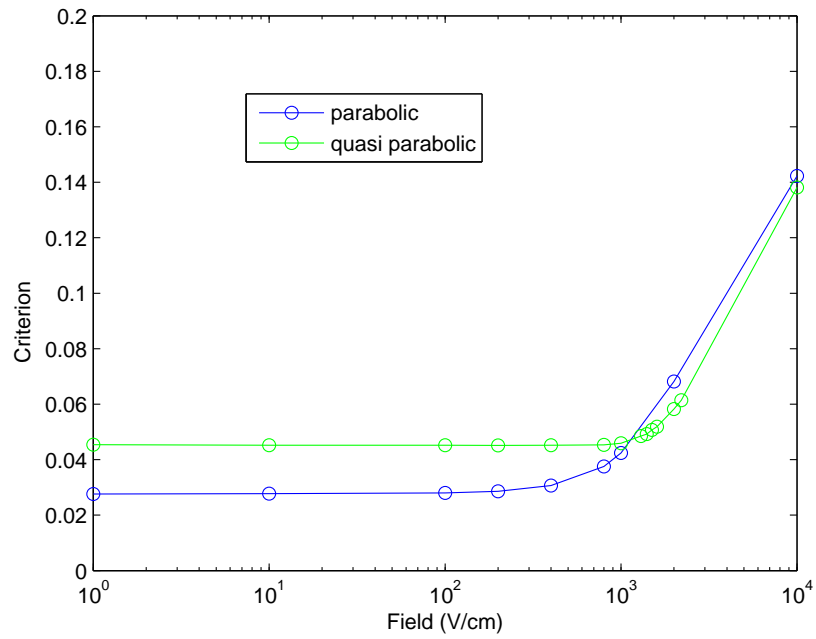


Figure 9: Steady state value of criterion (3.4) as a function of the electric field (bulk case, initial Maxwellian)

boundary region	energy (eV)	field (V/cm)
$x \in [0, 100]$	$0.04097 \pm 0.00003$	$-1265 \pm 28$
$x \in [650, 700]$	$0.04100 \pm 0.00008$	$-1278 \pm 25$

Table 7: Steady state values of energy and electric field averaged over boundary regions (cf. Figures 10, 11)

### 5.3 Diode

Here we consider a simple one-dimensional device called  $n^+ - n - n^+$  diode. The diode consists of two highly doped regions  $n^+$  (cathode and anode) connected by a less doped region  $n$  (channel). In order to avoid boundary effects, periodic boundary conditions are adopted so that an electron that exits through an interface is reinjected at the other end of the device. The quasi-parabolic band approximation (cf. (2.5)) is used.

The  $n^+$  regions are  $0.2 \mu\text{m}$  long and doped with a density of  $10^{19} \text{cm}^{-3}$ , while the channel is  $0.3 \mu\text{m}$  long and doped with a density of  $10^{18} \text{cm}^{-3}$ . The device is considered at room temperature  $T_L = 300 \text{K}$ . The applied voltage bias is  $3 \text{V}$ . The parameters  $N = 112000$  and  $N_{\text{rep}} = 10$  are used. The functionals are averaged between  $10 \text{ps}$  and  $20 \text{ps}$ , with an observation time step of  $0.1 \text{ps}$ .

The results for the energy and the electric field are displayed in Figures 10, 11. Results for the kurtosis and the criterion are given in Figures 12, 13. These observations provide a quantitative illustration of the statement that considerable parts of the boundary regions can be treated as spatially homogeneous. In Table 7 the macroscopic quantities are evaluated with additional averaging in the regions  $[0, 100 \text{nm}]$  and  $[650 \text{nm}, 700 \text{nm}]$ . It is observed that the energy estimates are consistent (in the sense of confidence intervals) with those obtained in the bulk case with an electric field of  $1300 \text{V/cm}$  as given in Table 6.

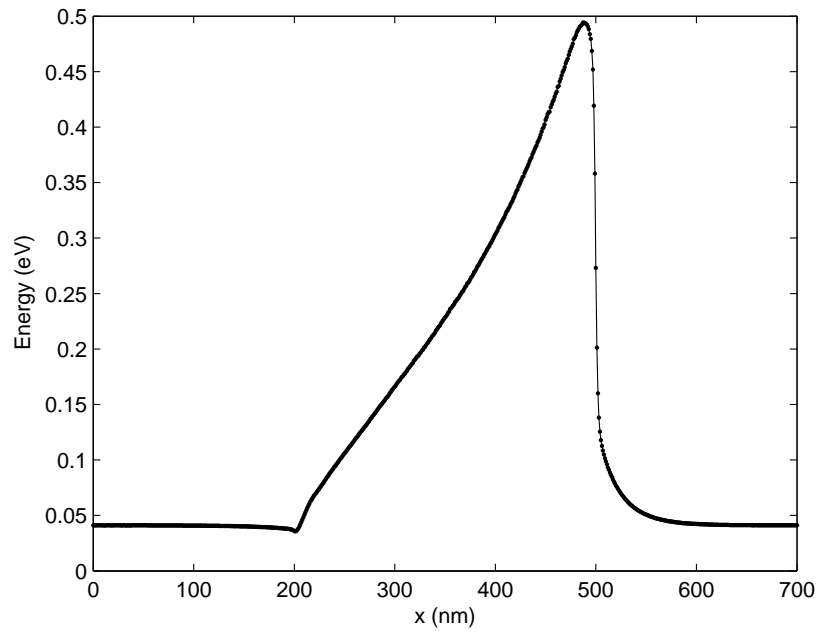


Figure 10: Average energy in the device (quasi-parabolic band, periodic boundary condition)

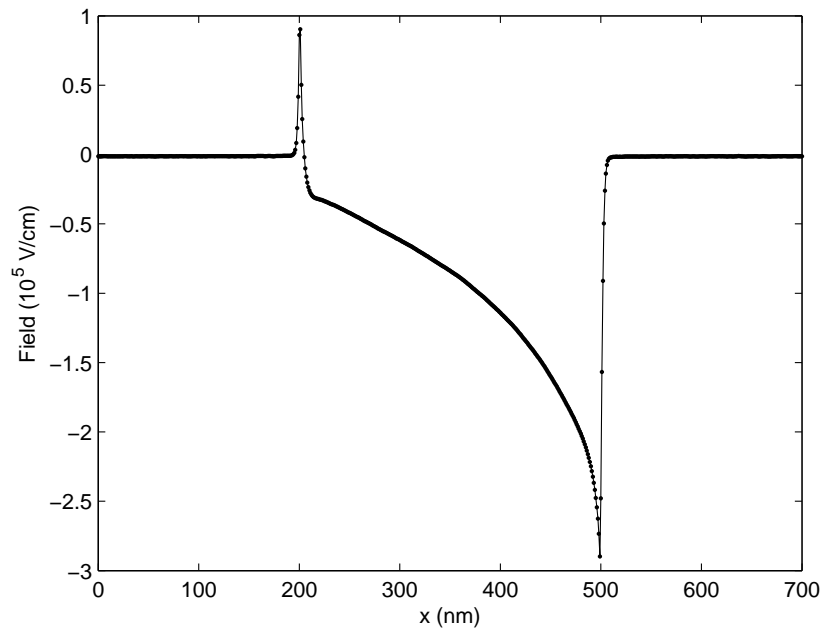


Figure 11: Average electric field in the device (quasi-parabolic band, periodic boundary condition)

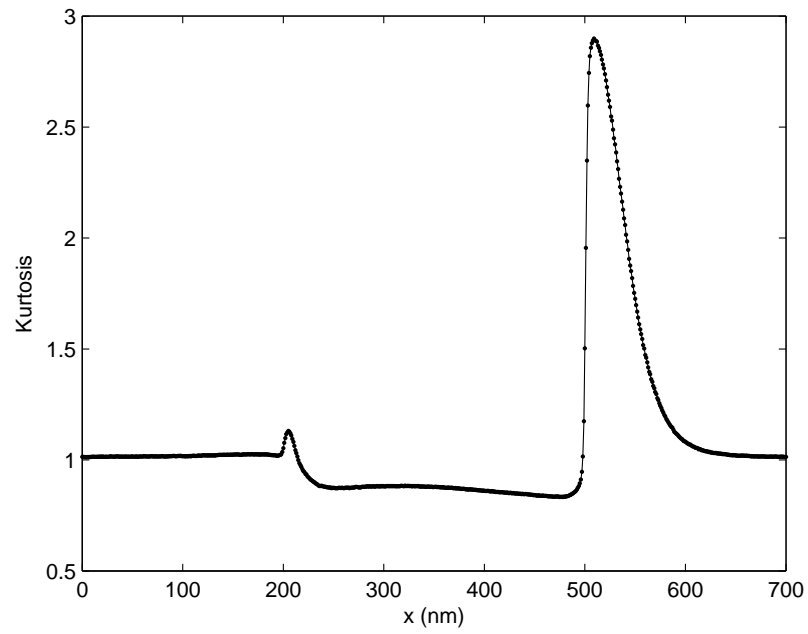


Figure 12: Kurtosis (3.3) in the device (quasi-parabolic band, periodic boundary condition)

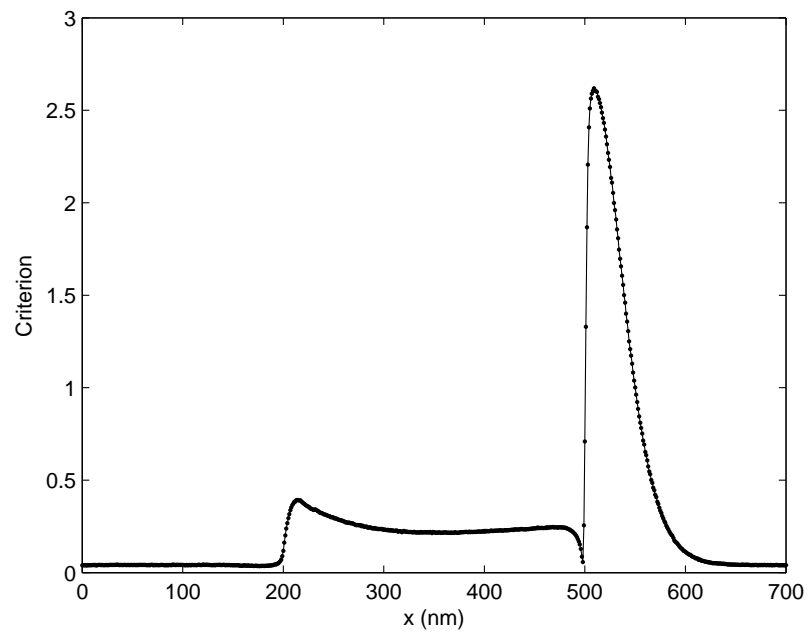


Figure 13: Criterion (3.4) in the device (quasi-parabolic band, periodic boundary condition)



## 6 Comments

The numerical experiments in the spatially homogeneous (bulk) case illustrate the theoretical results mentioned in Section 3.1. Moreover, they suggest several directions for further studies. For example, it would be of interest

- to characterize the steady state of the electron distribution function, when more than one scattering mechanism is involved, and
- to find conditions assuring that the Maxwellian with the lattice temperature is the unique steady state.

The numerical observations for the spatially one-dimensional test case (diode) provide a quantitative check of the statement that considerable parts of the boundary regions can be treated as spatially homogeneous. The extension of these studies to cases with more than one spatial dimension is straightforward. The information about the properties of the steady state electron distribution in the boundary regions might be useful for domain decomposition methods, or for improving the efficiency of modelling various boundary conditions.

It turned out that nonlinear functionals (as kurtosis and criterion) provide rather precise measurements of deviations from a given distribution function. For this particular purpose they are more appropriate than, for example, histograms. This methodology is applicable to other kinetic equations for semiconductors (cf., e.g., [4]), where the Maxwellian (3.1) is replaced by the Fermi-Dirac distribution (cf., e.g., [11]).

## Acknowledgements

The first and last authors have been supported by "Progetti di ricerca di Ateneo", Università degli Studi di Catania, and the CINECA Award N. HP10CHSS93, 2010 for the availability of high performance computing resources and support.

## References

- [1] L. ARLOTTI, J. BANASIAK, AND F. L. CIAKE CIAKE, *Conservative and non-conservative Boltzmann-type models of semiconductor theory*, Math. Models Methods Appl. Sci., 16 (2006), pp. 1441–1468.
- [2] J. BANASIAK, *On well-posedness of a Boltzmann-like semiconductor model*, Math. Models Methods Appl. Sci., 13 (2003), pp. 875–892.
- [3] J. BANASIAK AND L. ARLOTTI, *Perturbations of positive semigroups with applications*, Springer, London, 2006.

- [4] N. BEN ABDALLAH AND P. DEGOND, *On a hierarchy of macroscopic models for semiconductors*, J. Math. Phys., 37 (1996), pp. 3306–3333.
- [5] M. V. FISCHETTI, S. E. LAUX, P. M. SOLOMON, AND A. KUMAR, *Thirty years of Monte Carlo simulations of electronic transport in semiconductors: Their relevance to science and mainstream VLSI technology*, Journal of Computational Electronics, 3 (2004), pp. 287–293.
- [6] T. GRASSER, H. KOSINA, M. GRITSCH, AND S. SELBERHERR, *Using six moments of Boltzmann’s transport equation for device simulation*, J. Appl. Phys., 90 (2001), pp. 2389–2396.
- [7] T. GRASSER, H. KOSINA, C. HEITZINGER, AND S. SELBERHERR, *Characterization of the hot electron distribution function using six moments*, J. Appl. Phys., 91 (2002), pp. 3869–3879.
- [8] C. JACOBONI AND P. LUGLI, *The Monte Carlo Method for Semiconductor Device Simulation*, Springer, New York, 1989.
- [9] C. JACOBONI AND L. REGGIANI, *The Monte Carlo method for the solution of charge transport in semiconductors with applications to covalent materials*, Rev. Modern Phys., 55 (1983), pp. 645–705.
- [10] C. JUNGEMANN AND B. MEINERZHAGEN, *Hierarchical Device Simulation. The Monte-Carlo Perspective*, Springer, Wien, 2003.
- [11] A. MAJORANA, *Equilibrium solutions of the non-linear Boltzmann equation for an electron gas in a semiconductor*, Nuovo Cimento B, 108 (1993), pp. 871–877.
- [12] ———, *Trend to equilibrium of electron gas in a semiconductor according to the Boltzmann equation*, Transport Theory Statist. Phys., 27 (1998), pp. 547–571.
- [13] A. MAJORANA AND C. MILAZZO, *Space homogeneous solutions of the linear semiconductor Boltzmann equation*, J. Math. Anal. Appl., 259 (2001), pp. 609–629.
- [14] O. MUSCATO, W. WAGNER, AND V. DI STEFANO, *Numerical study of the systematic error in Monte Carlo schemes for semiconductors*, ESAIM: M2AN, 44 (2010), pp. 1049–1068.
- [15] S. RJASANOW AND W. WAGNER, *Stochastic Numerics for the Boltzmann Equation*, Springer, Berlin, 2005.
- [16] V. SVERDLOV, E. UNGERSBOECK, H. KOSINA, AND S. SELBERHERR, *Current transport models for nanoscale semiconductor devices*, Materials Science and Engineering, R 58 (2008), pp. 228–270.